Catalysis Today 202 (2013) 63–69

Contents lists available at SciVerse ScienceDirect

Catalysis Today

journal homepage: www.elsevier.com/locate/cattod

Local structure of Co doped RuO_2 nanocrystalline electrocatalytic materials for chlorine and oxygen evolution

Valery Petrykin[a,*], Kateřina Macounová[a], Maki Okube[a,b], Sanjeev Mukerjee[c], Petr Krtil[a,*]

[a] J. Heyrovský Institute of Physical Chemistry, Academy of Sciences of the Czech Republic, v.v.i., Dolejškova 3, 18223 Prague, Czech Republic
[b] Materials and Structures Laboratory, Tokyo Institute of Technology, 4259 Nagatsuta, Midori, Yokohama 226-8503, Japan
[c] Department of Chemistry and Chemical Biology, Northeastern University, 360 Huntington Ave., Boston, MA, USA

ARTICLE INFO

Article history:
Received 4 January 2012
Received in revised form 20 March 2012
Accepted 22 March 2012
Available online 15 May 2012

Keywords:
Oxygen evolution
Chlorine evolution
Oxide
EXAFS

ABSTRACT

Nano-particulate Co doped ruthenium dioxide electrocatalysts of the general formula $Ru_{1-x}Co_xO_{2-y}$ ($0 < x \leq 0.3$) were prepared by a co-precipitation method. The electrocatalysts with $x < 0.2$ conform to a single phase nano-crystalline materials. On the local level the Co forms clusters dispersed in the original rutile-like matrix. The local environment of the Co conforms to a rutile model which preserves the cationic arrangement but suppresses the probability of the Ru–Ru and Co–Co neighbors along the shortest metal–metal bonds. The electrocatalytic activity of the synthesized $Ru_{1-x}Co_xO_{2-y}$ materials in oxygen evolution is comparable with that of the non-doped ruthenium dioxide and little depends on the actual Co content. In presence of chlorides the Co doped materials are more selective towards oxygen evolution compared with the non doped ruthenia. The enhanced oxygen evolution in the case of Co doped electrocatalysts can be attributed to a chemical recombination of surface confined oxo-species. The selectivity shift towards oxygen evolution can be linked with limited activity of the $Ru_{1-x}Co_xO_{2-y}$ materials in the chlorine evolution reaction which seems to be relatively weakly dependent on the chloride concentration.

1. Introduction

Water electrolysis [1] and chlor-alkali industry [2] represent the main applications of electronically conductive transition metal oxides. Despite successful exploration of systems based on RuO_2 or IrO_2 in practical electrolysers the fundamental understanding of the electrocatalytic activity of this class of materials in multi-electron transfer processes is still incomplete. The limited understanding is particularly evident if one addresses the issue of selectivity of this type of catalysts in oxygen evolution process if the electrolyzed solutions contain chlorides. Poor selectivity to the oxygen evolution observed on the common rutile type oxide catalysts represents one of the main obstacles preventing wide implementation of the so called hydrogen economy.

A general approach to control the oxygen or chlorine selectivity on rutile type oxides which has been presented recently [3] utilizes a systematic theoretical description of the electrocatalytic processes on the rutile type oxides based on density functional theory (DFT) calculations [4,5]. The DFT based thermodynamic analysis predicts that both electrode processes are strongly correlated on rutile type oxide surfaces. In the case of oxygen evolution, it is stated that the process proceeds preferentially via surface peroxide-route [4] when the formation of the surface oxo- or peroxo- species represents the rate limiting step. Extending the same DFT approach to chlorine evolution process one finds that the surface peroxo-groups simultaneously act as the active sites in chlorine evolution. The selectivity of the rutile type surface in oxygen evolution process and chlorine evolution process, therefore, reflects the competition between both processes for the same surface active site. The oxygen as well as chlorine evolution activity are predicted to be restricted to two penta-coordinated (so called *cus*) transition metal cations present on the surface with bonding distance of ca. 3 Å [3,5,6]. In the rutile structural type native to both RuO_2 and IrO_2 this bonding distance corresponds to cation stacking along the *c* axis. The selectivity of the surface towards chlorine evolution results from the oxidative attack of the Cl^- on the surface peroxo groups connecting these two transition metal atoms along [0 0 1] direction [5]. The molecular dimension of the proposed active sites (2–5 Å) stresses the relevance of the local structure characterization in elucidation of catalytic activity in contrast to, e.g. diffraction data. Synthetic modification of the surface cation stacking ought to effectively adjust the material's selectivity. With respect to the local nature of the proposed active site one can address the selectivity problem by modifying the local structure of the oxide electrocatalysts via heterovalent substitution.

* Corresponding authors. Tel.: +420 266053826; fax: +420 286582307.
E-mail addresses: Valery.Petrykin@jh-inst.cas.cz (V. Petrykin), Petr.Krtil@jh-inst.cas.cz (P. Krtil).

0920-5861/$ – see front matter © 2012 Elsevier B.V. All rights reserved.
http://dx.doi.org/10.1016/j.cattod.2012.03.075

Ruthenium dioxide based electrocatalysts doped with V [7], Sn [8], Co [8,9], Ni [10], Fe [11] and, particularly, with Zn [3] were reported previously and their selectivity behavior was addressed by combination of voltammetric experiments with differential electrochemical mass spectroscopy (DEMS). The local structure effects and their influence on the electrocatalytic behavior were studied just for Ni and Zn doped materials [3,6,9]. Local structures of these materials cannot be described within the conventional paradigm of random substitution of host atoms by the dopant. The cations of different chemical nature promote formation of specific inclusions within the host rutile lattice that may be characterized in terms of crystallographically different phases conforming to rock salt [10] or ilmenite [6] structural types.

This paper extends the previous studies linking the local structure with electrocatalytic activity of rutile type oxides on the materials in the Ru–Co–O ternary system. The extended X-ray-absorption fine structure (EXAFS) data of these catalytically active materials are used to qualify general trends observed in the parallel oxygen and chlorine evolution and to outline competition of both reactions for the available surface sites.

2. Experimental

2.1. Synthesis of $Ru_{1-x}Co_xO_{2-y}$

The synthesis of Co doped ruthenia samples was attempted by Pechini and coprecipitation techniques. The coprecipitation route followed the procedure described previously [9,12,13]. The starting solutions of ruthenium(III) nitrosylnitrate (98%, Alpha Aesar) and cobalt (II) nitrate hexahydrate (99.999% Aldrich) in mixture of ethanol and propane-2-ol (1:1) (both Aldrich, ACS grade) were mixed with aqueous solution of tetramethylammonium hydroxide (25% Alpha Aesar) [13] to obtain hydroxide precipitates. The starting solutions contained both Ru and Co ions corresponding to the stoichiometry of the target oxides $Ru_{1-x}Co_xO_{2-y}$ ($x = 0.05, 0.10, 0.15, 0.20$ and 0.30). The precipitation procedure led to a formation of amorphous precursors, which were aged in a PTFE lined stainless steel autoclaves at 105 °C for 40 h. The washed and filtered powders were treated with hydrogen peroxide (1%), dried in air and annealed at 400 °C in air for 2 h to obtain nanocrystalline materials.

2.2. Characterization

The phase composition of the samples was analyzed by a Bruker D8 Advance powder X-ray diffractometer with Vantec-1 detector and $Cu_{K\alpha}$ radiation operating at 40 kV–30 mA in the scanning mode with a scanning rate of 1°/min. The XRD data for evaluation of lattice constants of $Ru_{1-x}Co_xO_{2-y}$ samples were collected in the step-scanning mode with 1 s/step using Ge powder as the internal standard. The bulk chemical composition of the prepared materials was analyzed by X-ray energy dispersive spectroscopy using Hitachi S4800 scanning electron microscope (SEM) equipped with a Nanotrace EDX detector (Thermo Electron). Particle sizes were based on the measurement of 200 randomly selected particles. The average particle size was found to be independent of the Co content and equals to 17 ± 4 nm. Correspondingly, the specific surface area was established assuming spherical approximation for the particle shape.

The X-ray absorption spectroscopy (XAS) was used to gather information on local structures of the materials in the vicinity of both Ru and Co atoms. X-ray near edge absorption spectra (XANES) and extended X-ray absorption fine structure (EXAFS) data were collected on pellets containing 20–30 mg of $Ru_{1-x}Co_xO_{2-y}$ in 200 mg of boron nitride (Aldrich, ACS grade) on X18B beam line (Si(1 1 1) monochromator) of the National Synchrotron Light Source (Brookhaven National Laboratory, USA). The spectra were measured in transmission mode at Ru K edge (22,117 eV) and Co K absorption edge (7709 eV). The Co K edge spectra of the sample with $x = 0.05$ were acquired in fluorescence mode using a 13 channel Ge detector. Each spectrum was recorded at three different scanning step sizes: pre-edge region from 200 to 30 eV was scanned in 5 eV steps to enable background subtraction; in the 30 eV pre-edge and 30 eV post-edge range the step size of 0.5 eV was used to acquire XANES part of the spectra, while the EXAFS data extending up to 16 $Å^{-1}$ in the k-space were collected with the variable step size corresponding to 0.05 $Å^{-1}$. Ru L3 absorption edge data (2838 eV) were collected at BL-11B beam line of Photon Factory (KEK, Japan) using the Si (1 1 1) monochromator, which provides $E/dE = 5000$ resolution. The powder samples were attached to the carbon tape and mount on the conducting sample holder. XAFS data were recorded in terms of total electron yield (TEY). Pre-edge range and XANES part of the spectra were recorded with 0.5 eV step size, while in the post edge range, the size of 5 eV was used.

The preliminary data handling, normalizations and extraction of the extended X-ray absorption fine structure (EXAFS) functions were performed in the IFEFFIT software package [14]. The photoelectron wave vector k for the Fourier transform of spectra was kept within the range of $k = 3.5–15.5$ $Å^{-1}$ for Ru-EXAFS and $k = 2–11.9$ $Å^{-1}$ for Co-EXAFS. The k-weighting factor of 2 was applied. The EXAFS functions are presented in R space in the range of $R = 1–6$ Å. The full-profile refinement of the EXAFS spectra by non-linear least squares (NLLS) minimization in the R-space with k-weighting factor equal to 2 was carried out using Artemis program of the IFEFFIT package. The theoretical models were generated using FEFF6.2 library.

The electrodes for electrochemical experiments were prepared from synthesized $Ru_{1-x}Co_xO_{2-y}$ materials by sedimentation of nanocrystalline powder from a water based suspension on Ti mesh (open area 20%, Goodfellow). The duration and number of the depositions were adjusted to obtain the surface coverage of about 1–2 mg/cm^2 of active oxide. The deposited layers were stabilized by annealing the electrodes for 20 min at 400 °C in air. The initial oxide suspensions were prepared in an ultrasound bath and contained approximately 5 g/L of $Ru_{1-x}Co_xO_{2-y}$ in MilliQ quality de-ionized water.

The electrochemical behavior of the $Ru_{1-x}Co_xO_{2-y}$ electrocatalysts was studied by potentiostatic as well as potentiodynamic techniques combined with differential electrochemical mass spectroscopy (DEMS). All experiments were performed in a home-made Kel-F single compartment cell. The experiments were performed in a three electrode arrangement using a PAR 263A potentiostat. Pt and Ag/AgCl were used as an auxiliary and a reference electrode, respectively. The reference electrode was connected via Luggin capillary to avoid chloride contamination. The activity of the prepared materials in both oxygen and chlorine evolution reactions was studied in 0.1 M $HClO_4$ (Aldrich, p.a.) containing variable amount of NaCl (Aldrich, ACS grade) corresponding to concentrations between 0.01 and 0.3 M. The DEMS apparatus consisted of Prisma™ QMS200 quadrupole mass spectrometer (Balzers) connected to TSU071E turbomolecular drag pumping station (Balzers).

3. Results and discussion

The powder XRD data of $Ru_{1-x}Co_xO_{2-y}$ ($0.05 \le x \le 0.30$) samples annealed at 400 °C are shown in Fig. 1. All samples are of a single-phase character. The reflection positions as well as intensities of diffraction peaks matched those of RuO_2 PDF file #431027. The volume of the unit cell, nevertheless, changes continuously in the range of $0 < x < 0.2$ (see Fig. 2) suggesting that the material with $x = 0.3$ may contain an amorphous secondary phase, which could

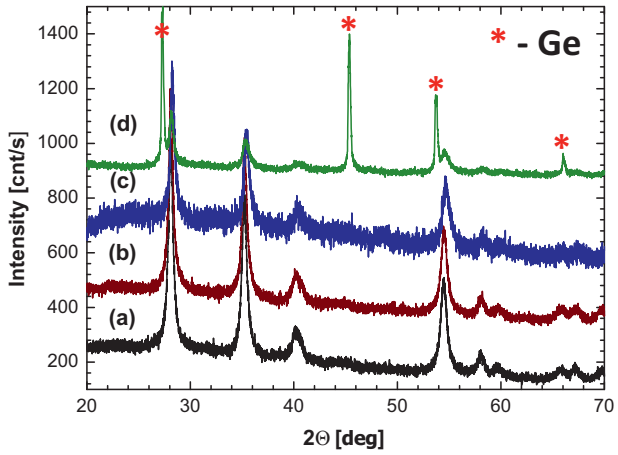

Fig. 1. Powder X-ray diffraction patterns of nanocrystalline $Ru_{1-x}Co_xO_{2-y}$ with x equal to 0.05 (a), 0.10 (b) 0.15 (c) and 0.20 (d) after annealing at 400 °C for 2 h.

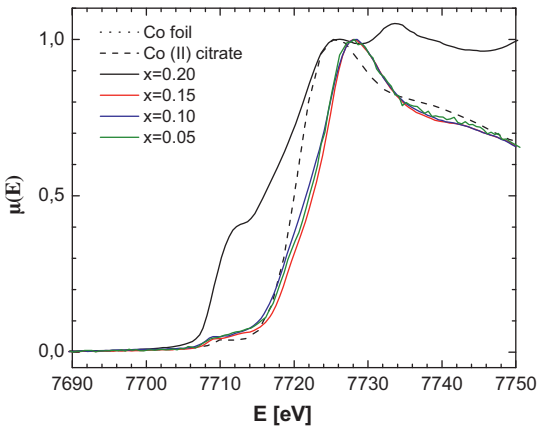

Fig. 3. Co K edge XANES data for $Ru_{1-x}Co_xO_{2-y}$ (x = 0.05–0.20) along with Co reference foil and Co(II) citrate reference. The actual curve assignment is given in figure legend.

not be identified by XRD. The materials with $x > 0.2$ were, therefore, not a subject of further characterization. The observed decrease of the unit cell volume with the increase of Co concentration suggests that cobalt oxidation state to be rather +3 than +2 as can be concluded from the literature based values of ionic radii (Ru^{+4}(0.62 Å), low spin Co^{+3} (0.55 Å) and low spin Co^{+2} (0.65 Å) [15].

In fact, the comparison of XANES parts of X-ray absorption spectra shows that position of the Co K-edge (7724 eV) in the whole composition range of $Ru_{1-x}Co_xO_{2-y}$ is shifted ~15 eV towards higher energies compared to Co metal reference foil (Fig. 3). The same Figure presents also XANES spectrum of Co(II) citrate [$Co(C_6H_7O_7)_2$] ($P2_12_12_1$ space group (lattice constants: a = 13.4452 Å, b = 5.9138 Å, c = 10.4153 Å))which was used as a reference of Co in oxidation state of +2. Its Co K edge position of 7720 eV is in a good agreement with the expected edge position in cobalt (II) complexes (7720.5–7721.5 eV) [16], while the absorption edge for Co(III) is expected at slightly higher energy of ~7727 eV [16]. The difference between literature data and the observed K-edge position in $Ru_{1-x}Co_xO_{2-y}$ can be attributed to a different Co environment in rutile host compared to coordination compounds such as $Co(acac)_3$, although it may also indicate more complex electron re-distribution between d-levels of Ru and Co ions in $Ru_{1-x}Co_xO_{2-y}$. More accurate probe of oxidation state can be provided by XANES parts of the Ru L3 edge spectra (see Fig. 4). The XANES spectra do not show significant variation of the shape or edge position. The L3 edge energy was found at 2836.5 eV for pure RuO_2 and the maximum deviation in the edge position of the Co doped samples did not exceed 0.1 eV. This shows that the ruthenium oxidation state remains constant in the whole range of compositions. The observed trend of composition independent average oxidation state of both ruthenium and cobalt differs from that observed in the case of Ni doped materials which show a systematic change in the oxidation state of Ni reflecting the content of the doping cation [17]. This fact implies an essential difference in the compensation of the lower charge of the doping cation and consequently different local environments of Ni and Co atoms in the RuO_2 host framework. It should also implicate qualitative difference in catalytic behavior of both types of doped ruthenia catalysts. Assuming that the electro-neutrality is achieved primarily by oxygen stoichiometry adjustment, one may expect the local distribution of Co in the doped ruthenia to resemble that of Zn in Zn doped RuO_2 electrocatalysts [11], i.e. an intergrowth of cobalt and ruthenium rich phases with fixed oxygen content in the rutile blocks.

The local structure of the $Ru_{1-x}Co_xO_{2-y}$ electrocatalysts was resolved from XAFS data measured at Ru K- and Co K edges. Fig. 5 presents Fourier transformed EXAFS functions extracted from Ru K edge data plotted in the R-space to emphasize the chemically relevant information. The Ru-EXAFS functions resemble those of non-doped RuO_2, which were discussed in detail in [17]. According to Ref. [17] one can assign the first peak at 1.95–2.00 Å to the scattering of photoelectrons by oxygen atoms forming RuO_6 octahedra. The second strong peak at ~3.0–3.1 Å originates mainly from

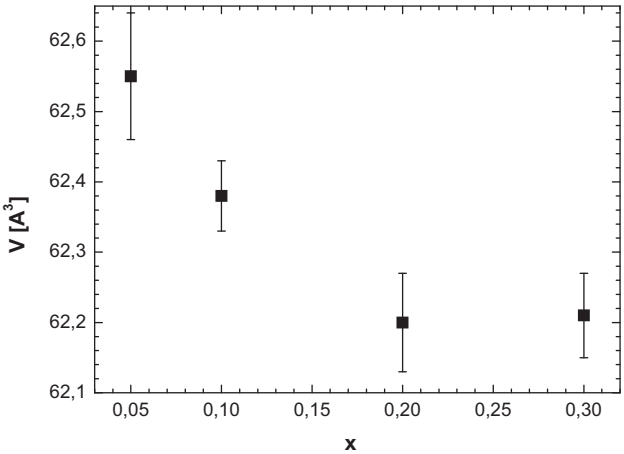

Fig. 2. Unit cell volume of the $Ru_{1-x}Co_xO_{2-y}$ catalysts as a function of the Co content.

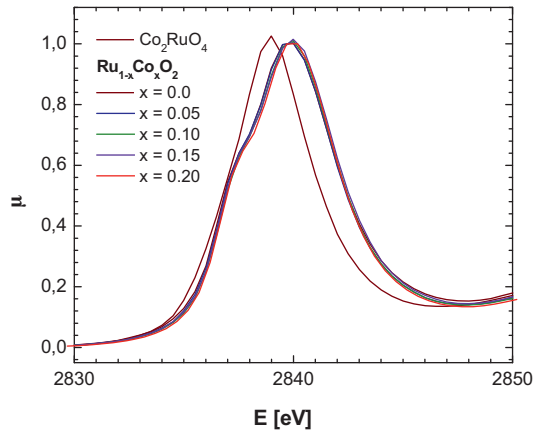

Fig. 4. Ru LIII edge XANES data for $Ru_{1-x}Co_xO_{2-y}$ (x = 0.00–0.20) materials. The spectrum of Co_2RuO_4 is included as a reference. The actual curve assignment is given in figure legend.

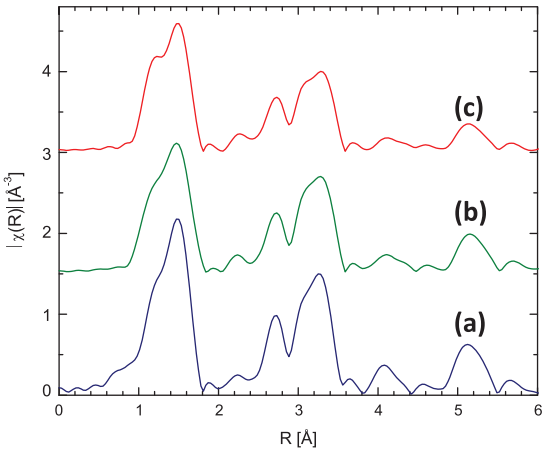

Fig. 5. k²-normalized RuK edge EXAFS functions of $Ru_{1-x}Co_xO_{2-y}$ (a) $x = 0.05$, (b) $x = 0.10$ and (c) $x = 0.15$.

the scattering process involving Ru–Ru path along the *c* axis of RuO_2 crystal. The next strong peak at 3.5–3.7 Å includes contributions from several scattering paths, while its main component reflects Ru–Ru coordination along the body diagonal of RuO_2 unit cell. As one may notice from the set of Ru-EXAFS functions in Fig. 5, introduction of Co into RuO_2 does not lead to significant changes of the local environment of Ru atoms since position of the peaks and their relative magnitude remain constant. The Co-EXAFS functions do resemble those recorded on the Ru K edge only in general features (see Fig. 6). The local environment of Co atoms is significantly altered compared to that in the rutile structure, mainly as far as the metal-metal coordination is concerned. Co EXAFS functions were refined using the strategy outlined in Ref. [17]. The results of the Co local structure refinement based on the collected Co-EXAFS data are summarized in Fig. 7 and in Table 1. In the beginning of the refinement the occupancy of different metal sites by cobalt was assumed to be equal and the fraction of Co atoms was fixed at 0.2, which is defined by the overall cobalt concentration in the material. In the final stages of the refinement this parameter was released and refined independently. The local environment

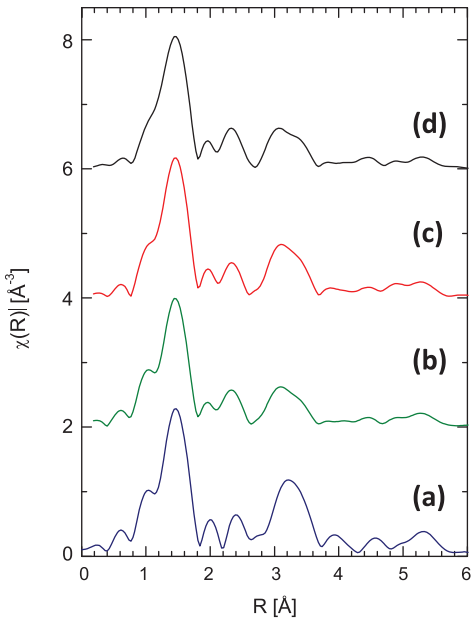

Fig. 6. k²-normalized Co-K EXAFS functions of $Ru_{1-x}Co_xO_{2-y}$ (a) $x = 0.05$, (b) $x = 0.10$, (c) $x = 0.15$ and (d) $x = 0.20$.

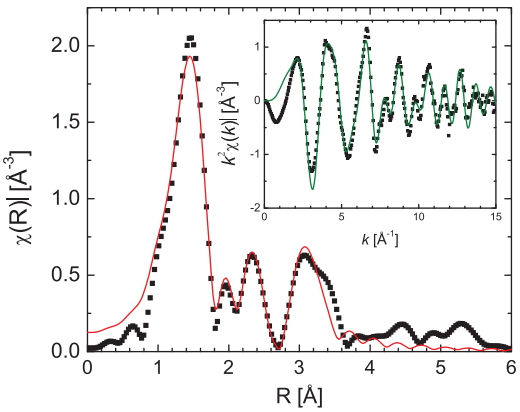

Fig. 7. k³-normalized Co-K EXAFS function for $Ru_{1-x}Co_xO_{2-y}$ $x = 0.20$ (square), and refinement result using rutile as a structural model. Inset shows the results of the fitting in *k*-space.

Table 1
Typical interatomic distances and Debye–Waller factors refined for the $Ru_{1-x}Co_xO_{2-y}$ oxide obtained by fitting the k²-normalized Fourier transformed EXAFS function for Co K edge (7709 eV) X-ray absorption spectrum. *R*-factor = 0.0157, *k* range 2.0–11.90 Å^{-1}, *R* range 1–4.5 Å, amplitude = 0.64(5), $E_0 = -3.84(76)$ eV. Multiple scattering paths are not shown.

Path	CN	Bond length (Å)	DW ($\times 10^3$ Å^2)
Co–O	2	1.87(2)	2.0(7)
	4	1.93(2)	
Co–Ru/Co[a]	2	3.05(5)	6.4(9)
Co–O	4	3.31(9)	2.0(7)
Co–Ru/Co[b]	8	3.52(1)	6.4(9)
Co–O	4	3.54(10)	2.0(7)
Co–O	8	3.91(11)	2.0(7)
Co–Ru/Co[b]	4	4.46(3)	6.4(9)

[a] Refined occupancy of Ru site by Co is −0.13(14). The value was fixed at 0.0.
[b] Refined occupancy of Ru site by Co is 0.18(8).

of Co does not show any variance with actual Co content. Table 1 shows that the obtained Co—O distances of 1.87 and 1.93 Å are considerably shorter than Ru—O bond length of 1.93 and 1.99 Å in the conventional RuO_2. This result is consistent with the XRD and XANES data, which suggest cobalt oxidation state in these materials to be +3. Consequently, one should expect contraction of CoO_6 octahedra due to 0.07 Å smaller ionic radius of Co^{3+} compared to Ru^{4+}. The most surprising feature of the refined local structure is connected with the fact that the fraction of Co in the neighboring metal sites along *c* axis of the unit cell is essentially zero, while most of the cobalt ions are located along body diagonal of the unit cell. This atomic arrangement (reflected by data in Table 1) is schematically depicted in Fig. 8. The atomic arrangement in such a cluster preserves the architecture of the rutile lattice. The sequence of the Co and Ru atoms resembles the arrangement of the cations in the trirutile lattice (AB_2O_6) such as $CrTa_2O_6$ in which crystallographic ordering of cations leads to the tripling of the unit cell. The

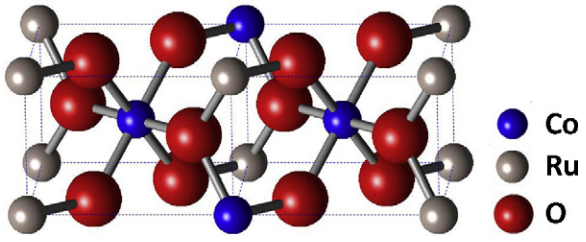

Fig. 8. Schematic representation of the Co cluster architectures based on refinement of EXAFS functions measured on $Ru_{1-x}Co_xO_{2-y}$ ($x = 0.20$).

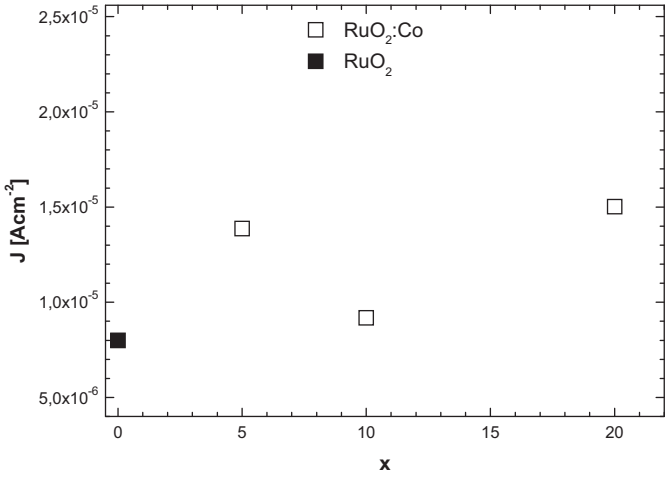

Fig. 9. Oxygen evolution activity of the $Ru_{1-x}Co_xO_{2-y}$ ($0 < x < 0.2$) as a function of Co content. The activity values were extracted from linear scan voltammetry in 0.1 M $HClO_4$ as the value of current density at 1.2 V (vs. SCE). The experiments were carried out at the scan rate of 5 mV/s.

XRD or electron diffraction patterns of $Ru_{1-x}Co_xO_{2-y}$ materials are, however, free of additional reflections indicating the absence of the long range translation symmetry of such clusters. Hereinafter, this type of clusters will be refered to as pseudo-rutile in the text. The very similar arrangement of doping atoms was observed in Ni doped RuO_2 nanostructured electrocatalysts with Ni content as low as 5%. While the Ni doped materials undergo continuous development of the local at higher concentrations of nickel forming Ni-rich shear planes at high degree of doping [17]. The EXAFS data for Co doped materials clearly show that the same architecture of the cluster remains unchanged till as high Co content as $x = 0.20$ in $Ru_{1-x}Co_xO_{2-y}$ materials.

The prepared Co doped ruthenia are active catalysts for anodic gas evolution in acid media. The electrocatalytic activity and selectivity of the synthesized $Ru_{1-x}Co_xO_{2-y}$ materials in OER and CER processes are summarized in Figs. 9–12. The actual oxygen evolution activity shows negligible dependence on the actual Co content (see Fig. 9). This behavior is opposite to that observed previously for Ni [18] or Fe [11] doped materials and is in general agreement with the local structure reported above. In the case of the Co doped ruthenia the electrocatalysts essentially comply with the rutile structural model for both types of transition metal cations – Ru and Co. Consequently, the introduction of Co rich pseudo-rutile regions is not likely to alter substantially the cation stacking in the direction relevant to the electrocatalytic activity in oxygen ((0 0 1) direction). The structural similarity of the original Ru rich rutile blocks and introduced pseudo-rutile Co containing regions suggests that the intrinsic activity of both types of regions which may be present at the catalysts surface may be comparable resulting in the observed composition-independence of the catalytic activity in the oxygen evolution reaction.

Fundamentally the same trend can be tracked in selectivity behavior in the parallel chlorine and oxygen evolution on $Ru_{1-x}Co_xO_{2-y}$ electrocatalysts with variable Co content (see Figs. 10–12). Typical response of the $Ru_{1-x}Co_xO_{2-y}$ catalysts to a potential step perturbation in the parallel oxygen and chlorine evolution is shown in Fig. 10. The data present in Fig. 10 clearly show, that an application of sufficiently positive potential (at which both gases can be thermodynamically evolved) results in immediate detection of produced chlorine. The chlorine evolution is not accompanied by oxygen evolution in the initial stages of the experiment. The electrocatalytically evolved oxygen can be detected with a time delay which decreases from ca. 20 s at 1.10 V to about 2 s at

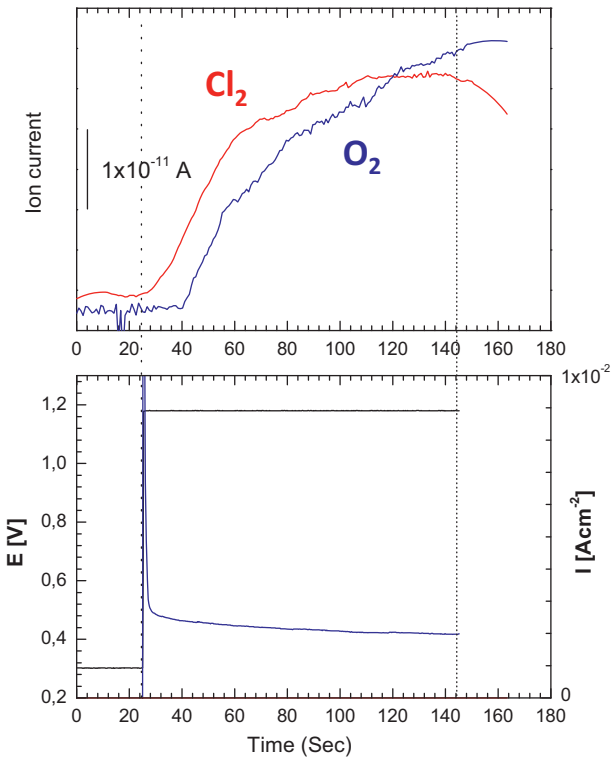

Fig. 10. Top: time course of DEMS based signals reflecting oxygen (blue) and chlorine (red) evolution on $Ru_{1-x}Co_xO_{2-y}$ ($x = 0.2$) in O.1 M $HClO_4$/0.05 M NaCl during potential step experiment at 1.2 V. Bottom: electric characteristics of the corresponding chronoamperometric experiment. Vertical lines mark the beginning and end of the potential perturbation and were added to guide the eye. (For interpretation of the references to color in this figure legend, the reader is referred to the web version of this article.)

1.3 V. The chlorine related signal attains a constant value within 1 min of the experiment regardless of the course of the oxygen evolution. The constant value the chlorine related DEMS signal represents a situation when the rate of the chlorine production (which ought to reflect only fluctuations in the chloride concentration) equals the rate of the chlorine transfer from the electrochemical cell into vacuum system. The constant chlorine production signal therefore rules out a transport limitation of the chlorine related current even at rather low chloride concentration of 0.05 M at the timescale of the experiment.

The oxygen evolution signal on the other hand fails to reach a steady state when the rate of oxygen production would be compensated by the removal into vacuum system. The observed increase of the oxygen evolution signal even after removing the potential perturbation indicates that the oxygen evolution is likely to be kinetically controlled by a process of chemical nature like, e.g. surface recombination, from previously accumulated reaction intermediates. Crystal edge facilitated recombination of surface confined oxo species [7] can be viewed as such an alternative mechanism. This reaction path has not been generally involved in the DFT calculations [4,5] although the recombination may successfully compete with peroxo route for ruthenium based oxides [19]. The same qualitative behavior is observed regardless of the actual Co content.

The selectivity of the $Ru_{1-x}Co_xO_{2-y}$ catalysts, changes with increasing Co content as well as with the applied potential. The high selectivity towards chlorine evolution observed for non-doped ruthenium dioxide gradually changes towards oxygen evolution with increasing Co content and becomes Co content independent when the fraction of cationic positions occupied by Co exceeds 0.1 (see Fig. 12). The chlorine evolution extent initially increases

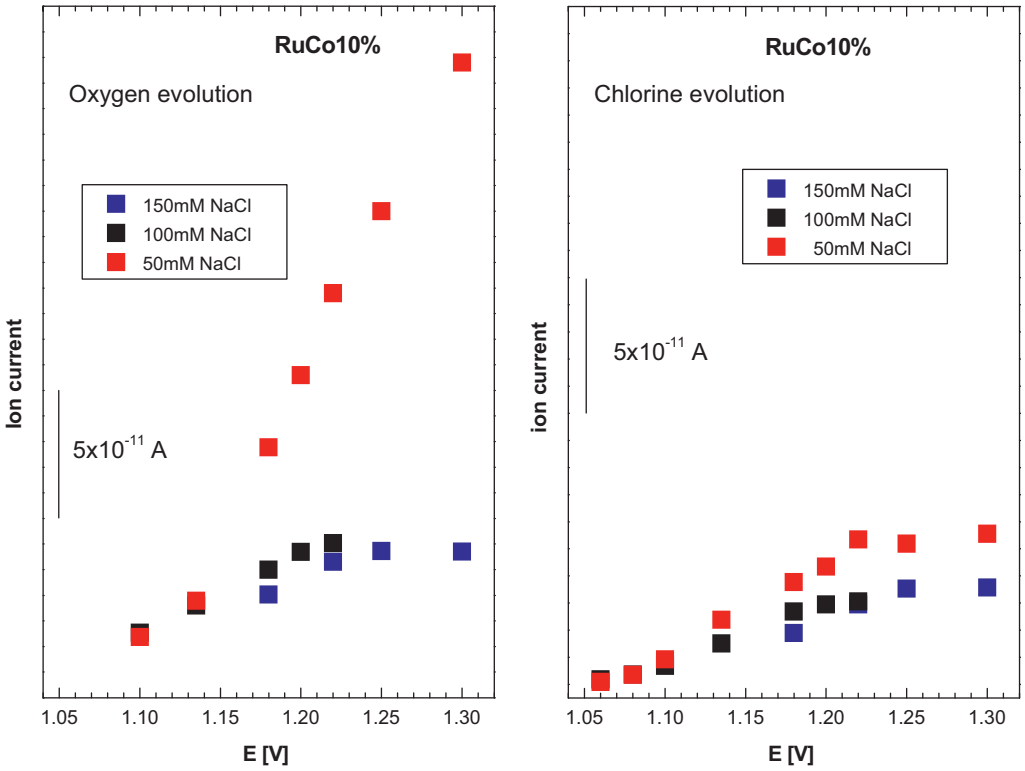

Fig. 11. Potential dependence of the DEMS based signals of the oxygen evolution (left) and chlorine evolution (right) in potentiostatic parallel oxygen and chlorine evolution in 0.1 M $HClO_4$ containing different concentration of NaCl. The actual NaCl concentration is shown in figure legend. The values represent a steady state DEMS readings on channels with m/z of 32 (oxygen) and 70 (chlorine) 90 s after potential perturbation.

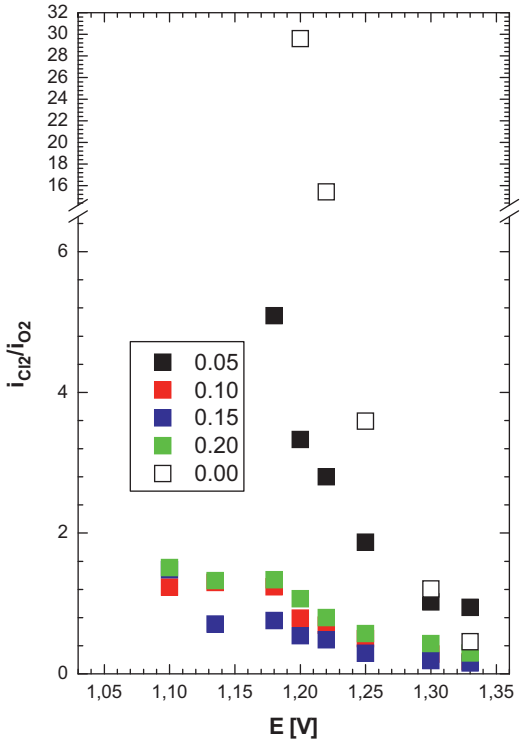

Fig. 12. Potential dependence of the DEMS based selectivity i_{cl}/i_o of the Co doped ruthenia catalysts and non-doped RuO_2 in parallel oxygen and chlorine evolution in 0.1 M H legend ClO_4 containing 0.05 M of NaCl. The assignment of the symbols is given in the figure.

with potential and reaches a steady state value at potentials of ca. 1.2 V. The extent of the oxygen evolution process, reflected by the DEMS, increases with applied potential and surpasses the chlorine evolution at potentials around 1.2 V. This type of behavior can be ascribed to different mechanism of the oxygen evolution below and above 1.2 V [20] resulting from the different intermediate surface coverage. The overall activity as well as selectivity of the $Ru_{1-x}Co_xO_{2-y}$ electrocatalysts seems to be little dependent on the chloride content in the concentration range 0.05–0.150 M (see Figs. 11 and 12). This finding seems to be in accordance with the fact that the actual extent of the chlorine evolution on the $Ru_{1-x}Co_xO_{2-y}$ surfaces can be sustained by relatively moderate 50 mM concentration of chlorides and the chlorine evolution process then seems to be intrinsically limited by the catalysts surface.

Similarly, a shift in the selectivity of ruthenium based oxides in favor of oxygen evolution has been reported for the Zn doped ruthenia [3,6]. The Zn doped ruthenia show a low activity in chlorine evolution due to the absence of the active sites needed to form surface peroxides – the key active site for both oxygen as well as chlorine evolution. The Co doped materials show more complex behavior in which the active sites needed for surface peroxo intermediate formation are still present. The nature of the Co distribution in the pseudo-rutile environment shows a pronounced tendency of Co to pair with the bonding distance of about 3.5 Å (i.e. along the body diagonal) and virtually zero probability of Co pairing with bonding distance of 3.1 Å (i.e. along the c axis). Since the body diagonal vector stands out of the {1 1 0} planes, then any Co residing in *cus* position must be free of any Co neighbors in the surface plane. Assuming that the Co distribution is free of further restrictions one can conclude that an increase of the the total Co content results in a disturbance of Ru–Ru sequences both in the *cus* as well as in *bridge* positions. In other words the probability of Ru in the *cus* position

to have Co neighbors in the *cus* positions increases with increasing Co content. Drawing an analogy from the behavior of the Ni doped ruthenia, where the Ni clustering suppresses cation alternation in *cus* positions enhances selectivity towards chlorine evolution [6], one can view the variation of Co and Ru in adjacent *cus* positions as a suppressor of the chlorine evolution on the Co doped ruthenia surfaces. The true nature of the observed selectivity effects needs to be, however, assessed in a separate in situ spectroelectrochemical study.

4. Conclusions

Nano-particulate Co doped ruthenium dioxide electrocatalysts of the general formula $Ru_{1-x}Co_xO_{2-y}$ with x ranging between 0 and 0.3 were prepared by a co-precipitation method. The electrocatalysts characterized by $x < 0.2$ conform to a single phase nano-crystalline materials. The materials with higher Co content although giving diffraction patterns conforming to single phase rutile are likely to represent a coexistence of nanocrystalline $Ru_{1-x}Co_xO_2$ phase with an amorphous phase. The local structures assessed by means of EXAFS suggest that the Co tends to form clusters dispersed in the original rutile-like matrix. The local structure of the Co in these clusters can be described using a rutile model which essentially preserves the cationic arrangement of RuO_2 with the specific arrangement of Ru and Co atoms except the Ru–Ru and Co–Co neighbors along the shortest metal–metal bonds. The electrocatalytic activity of the synthesized $Ru_{1-x}Co_xO_{2-y}$ materials in oxygen evolution is essentially comparable with that of the non-doped ruthenium dioxide and apparently does not depend on the actual Co content. In presence of chlorides the Co doped materials show higher selectivity towards oxygen evolution compared with the non doped ruthenia. The preference of the oxygen evolution process enhances with the potential as well with increasing Co content. The enhanced oxygen evolution in the case of Co doped electrocatalysts can be attributed to a chemical recombination of surface confined oxo-species. It represents an analogue of the Volmer–Tafel reaction sequence known in the case of hydrogen evolution. The selectivity shift towards oxygen evolution can be linked with limited activity of the $Ru_{1-x}Co_xO_{2-y}$ materials in the chlorine evolution reaction, which seems to be relatively weakly dependent on the chloride concentration. This type of behavior suggests that despite relative structural similarity of the Co rich and Ru rich environment (pseudo-rutile and rutile, respectively) the intrinsic selectivity of the active sites in each of the environment may differ with pseudo-rutile essentially preferring the oxygen evolution due to alternative stacking of the Co and Ru cations along the (0 0 1) direction relevant to the formation of the active sites.

Acknowledgements

This work was supported by the Academy of Sciences of the Czech Republic under contract KAN100400702 and by the Grant Agency of the Academy of Sciences of the Czech Republic under contract No. IAA400400906. VP acknowledges the support of the Marie Curie International Incoming Fellowship (IIF No. 220711) of the European Commission. The synchrotron measurement time was provided by National Synchrotron Light Source at Brookhaven National Laboratory (USA) Project No. 11734 and Photon Factory, KEK (Japan) Projects 2005G146 and 2010G569

References

[1] M.W. Kanan, D.G. Nocera, Science 321 (2008) 1072.
[2] S. Trasatti, Electrochimica Acta 45 (2000) 2377.
[3] V. Petrykin, K. Macounová, O. Shlyakhtin, P. Krtil, Angewandte Chemie International Edition 49 (2010) 4813.
[4] J. Rossmeisl, Z.W. Qu, H. Zhu, G.J. Kroes, J.K. Norskov, Journal of Electroanalytical Chemistry 607 (2007) 83.
[5] H.A. Hansen, I.C. Man, F. Studt, F. Abild-Pedersen, T. Bligaard, J. Rossmeisl, Physical Chemistry Chemical Physics (2010) 283.
[6] V. Petrykin, K. Macounova, J. Franc, O. Shlyakhtin, M. Klementova, S. Mukerjee, P. Krtil, Chemistry of Materials 23 (2011) 200.
[7] W. Sugimoto, T. Shibutani, Y. Murakami, Y. Takasu, Electrochemical and Solid State Letters 5 (2002) A170–A177.
[8] (a) C.P. De Pauli, S. Trasatti, Journal of Electroanalytical Chemistry 538 (2002) 145;
(b) C.P. De Pauli, S. Trasatti, Journal of Electroanalytical Chemistry 396 (1995) 161;
(c) J. Gaudet, A.C. Tavares, S. Trasatti, D. Guay, Chemistry of Materials 17 (2005) 1570.
[9] (a) L.M. Da Silva, J.F.C. Boodts, L.A. De Faria, Electrochimica Acta 46 (2001) 1369;
(b) N. Krstajic, S. Trasatti, Journal of the Electrochemical Society 142 (1995) 2675;
(c) L.M. Da Silva, J.F.C. Boodts, L.A. De Faria, Electrochimica Acta 45 (2000) 2719;
(d) M. Makarova, J. Jirkovsky, M. Klementova, I. Jirka, K. Macounova, P. Krtil, Electrochimica Acta 53 (2008) 5626.
[10] K. Macounova, M. Makarova, J. Jirkovsky, J. Franc, P. Krtil, Electrochimica Acta 53 (2008) 6126.
[11] K. Macounova, M. Makarova, J. Jirkovsky, J. Franc, P. Krtil, Electrochemical and Solid State Letters 11 (2008) F28.
[12] J. Jirkovsky, H. Hoffmannova, M. Klementova, P. Krtil, Journal of the Electrochemical Society 153 (2006) E111.
[13] S. Music, S. Popovic, M. Maljkovic, K. Furic, A. Gajovic, Materials Letters 56 (2002) 806.
[14] M. Neville, Journal of Synchrotron Radiation 8 (2001) 322.
[15] R.D. Shannon, Acta Crystallographica A 32 (1976) 751.
[16] P.D. Bonnitcha, M.D. Hall, C.K. Underwood, G.J. Foran, M. Zhang, P.J. Beale, T.W. Hambley, Journal of Inorganic Biochemistry 100 (2006) 963.
[17] V. Petrykin, Z. Bastl, J. Franc, K. Macounova, M. Makarova, S. Mukerjee, N. Ramaswamy, I. Spirovova, P. Krtil, Journal of Physical Chemistry C 113 (2009) 21657.
[18] K. Macounova, J. Jirkovsky, M.V. Makarova, J. Franc, P. Krtil, Journal of Solid State Electrochemistry 13 (2009) 959.
[19] K. Macounova, M. Makarova, P. Krtil, Electrochemistry Communications 11 (2009) 1865.
[20] J. Jirkovský, M. Busch, E. Ahlberg, P. Panas, Krtil, Journal of the American Chemical Society 133 (2011) 5882.